SSD-TR-92-11

AEROSPACE REPORT NO.
TR-92(2935)-2

AD-A253 383

Damage Modes and Mechanisms of Si-Ge Films Under Prompt Soft X-Ray Radiation

Prepared by

S. R. GYETVAY and D. J. CHANG
Mechanics and Materials Technology Center
Technology Operations
The Aerospace Corporation
El Segundo, CA 90245-4691

and

R. MUKI
Civil Engineering Department
University of California, Los Angeles, CA 90024

13 May 1992

DTIC
ELECTE
JUL 16 1992
S B D

Prepared for

SPACE SYSTEMS DIVISION
AIR FORCE SYSTEMS COMMAND
Los Angeles Air Force Base
P. O. Box 92960
Los Angeles, CA 90009-2960

Engineering and Technology Group

THE AEROSPACE CORPORATION
El Segundo, California

92-18851

APPROVED FOR PUBLIC RELEASE;
DISTRIBUTION UNLIMITED

92 7 15 104

This report was submitted by The Aerospace Corporation, El Segundo, CA 90245-4691, under Contract No. F04701-88-C-0089 with the Space Systems Division, P. O. Box 92960, Los Angeles, CA 90009-2960. It was reviewed and approved for The Aerospace Corporation by R. W. Fillers, Principal Director, Mechanics and Materials Technology Center. LT E. W. Xenakis was the project officer for the Mission-Oriented Investigation and Experimentation (MOIE) program.

This report has been reviewed by the Public Affairs Office (PAS) and is releasable to the National Technical Information Service (NTIS). At NTIS, it will be available to the general public, including foreign nationals.

This technical report has been reviewed and is approved for publication. Publication of this report does not constitute Air Force approval of the report's findings or conclusions. It is published only for the exchange and stimulation of ideas.

MARTIN K. WILLIAMS, Capt, USAF
MOIE Program Manager

EVAN W. XENAKIS, 1LT, USAF
MOIE Project Officer

UNCLASSIFIED

SECURITY CLASSIFICATION OF THIS PAGE

REPORT DOCUMENTATION PAGE

1a. REPORT SECURITY CLASSIFICATION Unclassified	1b. RESTRICTIVE MARKINGS
2a. SECURITY CLASSIFICATION AUTHORITY 2b. DECLASSIFICATION/DOWNGRADING SCHEDULE	3. DISTRIBUTION/AVAILABILITY OF REPORT Approved for public release; distribution unlimited
4. PERFORMING ORGANIZATION REPORT NUMBER(S) TR-92(2935)-2	5. MONITORING ORGANIZATION REPORT NUMBER(S) SSD-TR-92-11
6a. NAME OF PERFORMING ORGANIZATION The Aerospace Corporation Technology Operations 6b. OFFICE SYMBOL *(If applicable)*	7a. NAME OF MONITORING ORGANIZATION Space Systems Division Los Angeles Air Force Base
6c. ADDRESS *(City, State, and ZIP Code)* El Segundo, CA 90245-4691	7b. ADDRESS *(City, State, and ZIP Code)* Los Angeles Air Force Base Los Angeles, CA 90009-2960
8a. NAME OF FUNDING/SPONSORING ORGANIZATION 8b. OFFICE SYMBOL *(If applicable)*	9. PROCUREMENT INSTRUMENT IDENTIFICATION NUMBER F04701-88-C-0089
8c. ADDRESS *(City, State, and ZIP Code)*	10. SOURCE OF FUNDING NUMBERS PROGRAM ELEMENT NO. / PROJECT NO. / TASK NO. / WORK UNIT ACCESSION NO.

11. TITLE *(Include Security Classification)*

Damage Modes and Mechanisms of Si-Ge Films Under Prompt Soft X-Ray Radiation

12. PERSONAL AUTHOR(S) Gyetvay, Sandra R; Chang, Dick J. (The Aerospace Corporation); and Muki, Rokuro (University of California at Los Angeles)

13a. TYPE OF REPORT	13b. TIME COVERED	14. DATE OF REPORT *(Year, Month, Day)*	15. PAGE COUNT
	FROM _____ TO _____	1992, May 11	21

16. SUPPLEMENTARY NOTATION

17. COSATI CODES			18. SUBJECT TERMS *(Continue on reverse if necessary and identify by block number)*
FIELD	GROUP	SUB-GROUP	

19. ABSTRACT *(Continue on reverse if necessary and identify by block number)*

Thermal and residual stresses in films exposed to sudden temperature changes are analyzed based on an elastoplastic-brittle idealization of film response. The results thus obtained are used to explain qualitatively the damage mechanisms of various failure modes observed in Si-Ge film deposited on a single crystal Si substrate exposed to soft x-ray radiation for a short duration of time.

20. DISTRIBUTION/AVAILABILITY OF ABSTRACT [X] UNCLASSIFIED/UNLIMITED [ ] SAME AS RPT [ ] DTIC USERS	21. ABSTRACT SECURITY CLASSIFICATION Unclassified
22a. NAME OF RESPONSIBLE INDIVIDUAL	22b. TELEPHONE *(Include Area Code)* / 22c. OFFICE SYMBOL

DD FORM 1473, 84 MAR

83 APR edition may be used until exhausted
All other editions are obsolete

SECURITY CLASSIFICATION OF THIS PAGE

UNCLASSIFIED

CONTENTS

1. INTRODUCTION 3
2. DAMAGE MODES AND TEMPERATURE 7
3. ANALYSES OF RESIDUAL STRESS AND WRINKLING 9
4. DAMAGE MECHANISMS 17

REFERENCES 19

FIGURES

1. Damage modes of coating under krypton x rays with normalized fluence 4
2. Temperature distribution in the coated substrate (DLC/K) 8
3. Temperature distribution, T (ξ, 1) and $\sigma_{CM}(\xi)/\beta$ 11
4. Schematic distribution of stress at the instant of peak compressive yield region and residual stress 14
5. Residual stress distribution 16

TABLES

1. Threshold Fluence and Surface Temperature at the End of Radiation 7
2. Effective Yield Stress in Compression 18

DTIC QUALITY INSPECTED 2

Accession For
NTIS GRA&I ☑
DTIC TAB ☐
Unannounced ☐
Justification
By
Distribution/
Availability Codes
Dist | Avail and/or Special
A-1

1. INTRODUCTION

Some solid films are, by chance or design, exposed to a sudden large temperature gradient or prompt radiation such as x ray or laser which results in a large stress in the film. Damage assessment of such films is important in determining the allowable upper bound of the temperature or radiation exposure that the film can sustain.

Certain damage modes have been observed[1] in coated substrates exposed to prompt soft x-ray radiation. For a film of prescribed properties, there is a threshold fluence level of x rays below which no visible mechanical damage occurs. For a fluence level slightly higher than the threshold value, the damage modes of film are wrinkling and defect-initiated cracking. When the fluence levels are increased progressively, other damage modes such as uniform cracking and flaking occur and, eventually, melting or blowoff takes place at high fluence levels. The objective of this report is to supply a qualitative explanation of the mechanisms of the damage modes observed at low fluence levels, namely, wrinkling, defect-initiated cracking, and uniform cracking.

In Section 2, we summarize the observations and results in Reference 1, which discusses failure diagnostics of coated single crystal Si substrates exposed to soft x-ray radiation of various fluence levels (cal/cm^2) over a short duration of time (22 nsec). Two types of coating of the same thickness (2.625 μm) were used: (a) a discrete-layered coating consisting of 10 pairs of distinct Si–Ge layers and (b) a rugate coating consisting of 10 pairs of continuously varying cycles.

The temperature distribution was evaluated in Reference 1 by taking the thermal characteristics of x-ray radiation and the temperature-dependence of material properties into account. We observed that the classical instantaneous heat source solution for the one-dimensional entire space captures the essential feature of the numerically predicted temperature distribution after krypton x-ray radiation. We therefore employed the classical heat source solution to represent the temperature distribution for thermal and residual stress analysis in the coating. Typical photographs of these damage modes, shown in Figure 1, are reproduced from Reference 1.

In Section 3, we formulate the idealized thermal and residual stress problem for the coating to supply a basis for explanation of damage modes of coating observed for low fluence levels. We regard the coating to be a homogeneous elastoplastic material with temperature-independent material properties bonded on a rigid substrate. The thermal and residual stresses due to the classical instantaneous heat source solution are then determined analytically. We also consider the idealization in which the coating material yields for compression, but breaks at a certain critical tensile stress. For ranges of fluence, the patterns of residual stress distribution and the expressions of crack depth are presented.

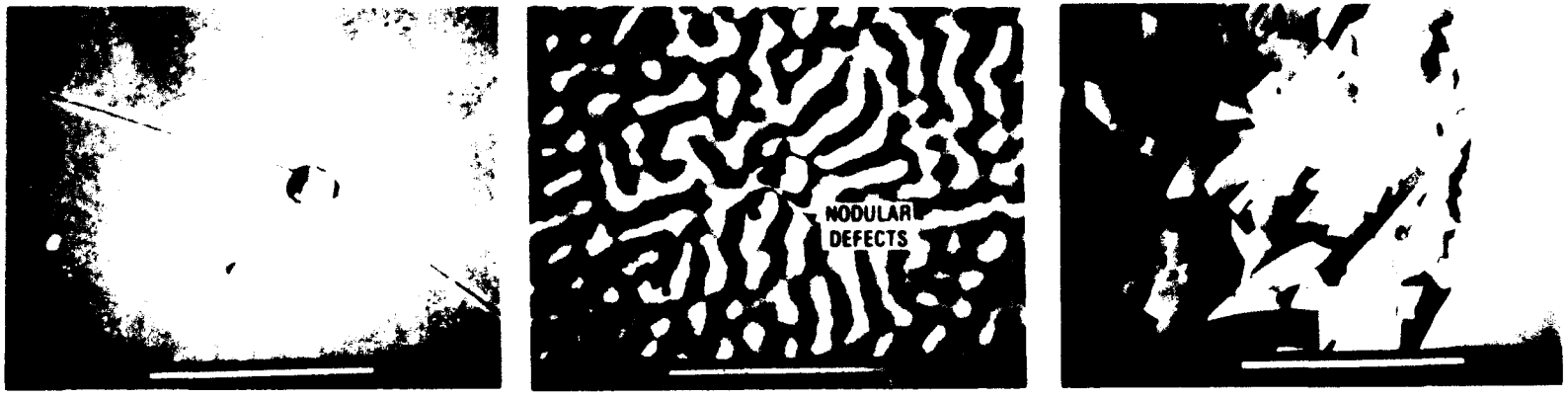

	(a) DEFECT-INITIATED CRACKING	(b) WRINKLING	(c) UNIFORM CRACKING
DLC	1.33 ~ 1.70	1.70	2.40 ~ 3.50
RC	1.70	–	2.40 ~ 3.50

Figure 1. Damage modes of coating under krypton x rays with normalized fluence: The white bar at the bottom is 10 μm long for (a), (b), and 1 nm for (c).

Finally, for the wrinkling damage mechanism observed in the discrete-layered coating, we regard the first few layers of the coating soon after x-ray radiation as an elastic plate with biaxial compression lying on an elastic foundation and show a model mechanism of the wrinkling damage mode.

In Section 4, we provide a qualitative explanation of each damage mode under prompt soft krypton x-ray exposure of low fluence levels based on the analysis in Section 3. We note that the wrinkling occurs due to biaxial compression of the top layers during or immediately after x-ray radiation, while the defect-initiated cracking and uniform cracking are caused by residual tensile stress which developed during and after the specimen cools down. We also supply a theoretical justification of the experimentally observed fact that the fluence for the uniform-cracking mode is twice the fluence for the defect-initiated cracking mode.

2. DAMAGE MODES AND TEMPERATURE

Experiments have been carried out for two types of coating on a single crystal Si substrate of thickness 3.175 mm exposed to two spectra of x ray (krypton, argon) of various fluence levels (cal/cm^2) for a pulse length of 22 nsec. Each coating has a thickness of 2.625 μm; one type of coating consists of 10 pairs of distinct Si-Ge layers (discrete-layered coating; DLC), while another consists of 10 pairs of continuously varying Si-Ge cycles (rugate coating; RC). Four combinations of the two coatings and two x-ray spectra will be denoted by DLC/K, RC/K, and DLC/A, RC/A.

Table 1 shows the highest fluence, F_o, without mechanical damage, and the surface temperature, T_o, at the end of radiation for each of the four combinations. We call F_o the threshold fluence.

The lower threshold values for the discrete-layered coating than those for the rugate coating may be attributed to the presence of material discontinuities between the Si and Ge sublayers; in the rugate coating, material composition changes continuously and there are no distinct interfaces. The higher threshold fluence for argon irradiation reflects its deeper penetration into the specimen, resulting in a more even and lower surface temperature distribution at the end of the radiation period than the counterparts exposed to krypton x rays.

For krypton radiation, the profile of the temperature distribution in the specimen after the exposure period is captured fairly accurately by the classical heat source solution as will be shown later. The use of the classical solution to represent the temperature in the specimen, in turn, greatly facilitates the analysis of residual stress. We therefore focus our discussion on the damage modes under krypton radiation. We define "normalized fluence" as the ratio of fluence to the threshold fluence listed in Table 1 and use it to identify the range in which each of the three damage modes was observed. The defect-initiated cracking shown in Figure 1(a) was observed for the normalized fluence as slightly larger than unity. Two new modes of damage were observed at higher fluences; wrinkling as shown in Figure 1(b) and uniform cracking as shown in Figure 1(c)

Table 1. Threshold Fluence and Surface Temperature at the End of Radiation

	Krypton		Argon	
Coating Type	F_o cal/cm^2	T_o °C	F_o cal/cm^2	T_o °C
DLC	0.030	339	0.119	582
RC	0.040	539	0.128	636

Temperature distributions in the specimen have been calculated numerically by taking x-ray absorption and temperature-dependent material properties into account using an Aerospace thermal diffusion deposition code (GENRAT/DEAP). The numerically generated temperature profiles for the discrete-layered coating under krypton radiation with fluence of 0.05 cal/cm^2 is shown by dashed curves in Figure 2, where the wavy character of the curves in the film is due to the discrete-layer composition of the film. It should be noted that the essential feature of the profile is captured by the classical heat source solution with the same surface temperature at the end of x-ray exposure, t = 22 nsec, and with the diffusivity κ = 0.3 cm^2/sec, as shown by solid curves. Supported by this observation, we assume, in the residual stress analysis, that the temperature distribution in the specimen is given by the classical solution, Eq. (1), where T_o is the numerically generated surface temperature at the end of irradiation, $t = t_o$.

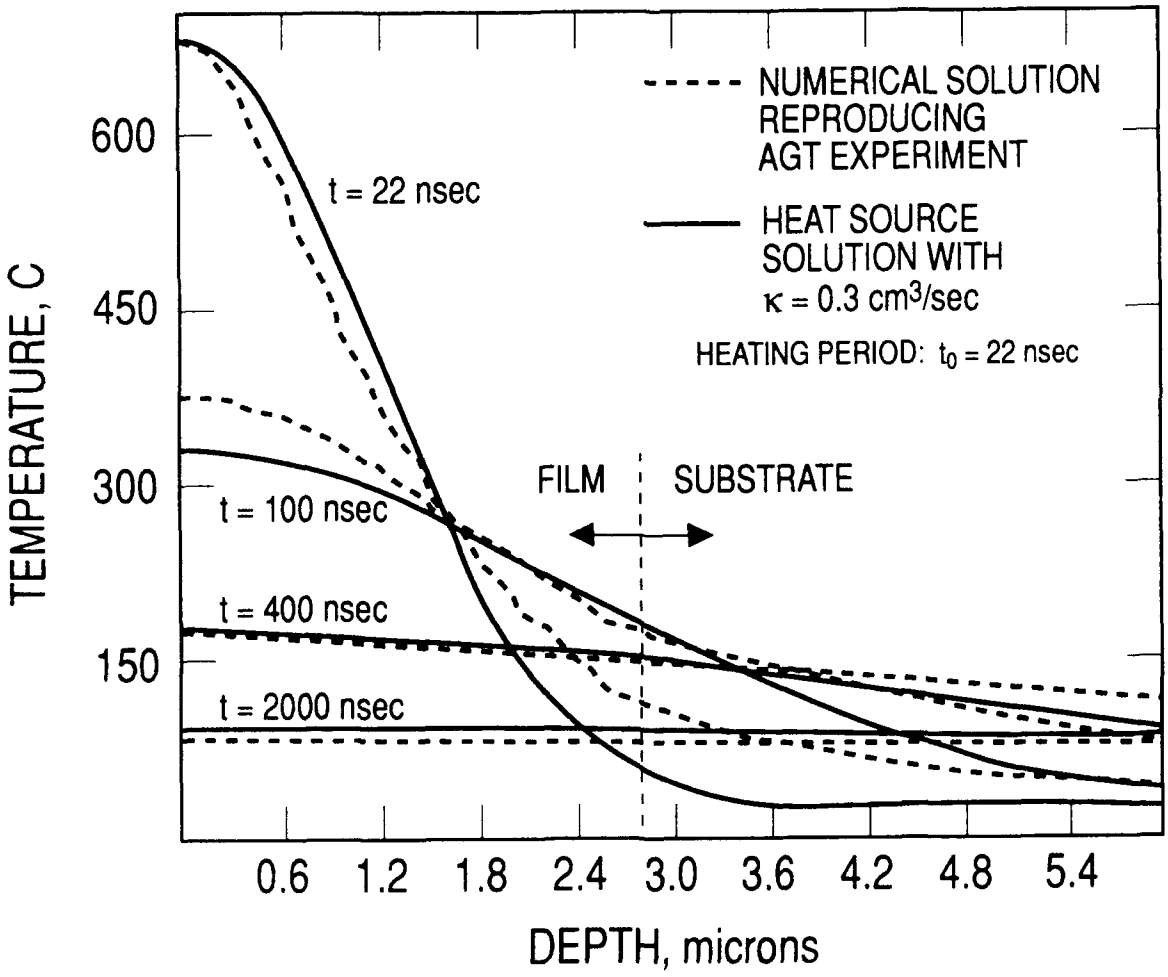

Figure 2. Temperature distribution in the coated substrate (DLC/K).

3. ANALYSES OF RESIDUAL STRESS AND WRINKLING

Suppose that a film of thickness d, deposited on a substrate of thickness h, where h > > d, is exposed to an intense heating for a short period of time, t_o. We assume that the film and substrate have the same value, κ, for the diffusivities, and the temperature distribution after the heating period is adequately represented by instantaneous heat source solution in an infinite solid:[2]

$$\bar{T}(x,t) = T_o \sqrt{\frac{t_o}{t}} \exp\left(-\frac{x^2}{4\kappa t}\right) \qquad (t_o < t < \infty) \tag{1}$$

where $x = 0$ denotes the surface with positive x toward the interior of the specimen and T_o is the surface temperature rise above the reference temperature at $t = t_o$.

Stress in the film can be regarded biaxially hydrostatic and it consists of intrinsic, thermal, and residual stresses. Intrinsic stress may be tensile or compressive depending upon the material and manufacturing process. In this analysis, we assume that the intrinsic stress is null. However, its effect can readily be taken into account.

Due to the extremely short duration of x-ray exposure and the thinness of the film, the greatest stress in the film occurs during the very short initial period. The lateral dimension of the film is much larger than the film thickness and we confine our attention to the portion away from the edge of the deposited film. Under this condition, one can show that stress in the substrate is of the order O(d/h) of the film stress and the effect of film-substrate interaction on the film stress can be safely disregarded. Based on the above observation, we regard the substrate as a rigid body in the analysis.

We adopt a model for mechanical response of film material:

Elastoplastic in compression and elasto-brittle (elastoplastic-brittle) in tension with Young's modulus E, Poisson's ratio ν, compressive equal-biaxial yield stress Y, and tensile strength S.

Following the assumption introduced above, the state of stress in the film is given by

$$\sigma_{xx} = 0 , \qquad \sigma_{yy} = \sigma_{zz} = \bar{\sigma}(x,t) \tag{2}$$

For elastic ranges, the thermal stress due to the temperature field, Eq. (1), becomes

$$\bar{\sigma}(x,t) = -\frac{\alpha \bar{T} E}{1-\nu} = -\frac{\alpha T_o E}{1-\nu} \sqrt{\frac{t_o}{t}} \exp\left(-\frac{x^2}{4\kappa t}\right) \tag{3}$$

where α is the coefficient of thermal expansion. At this point, dimensionless variables are introduced by

$$\left.\begin{aligned} \tau &= t/t_o\,, \qquad \xi = x/\sqrt{4\kappa t_o}\,, \\ T &= \bar{T}/T_o\,, \qquad \sigma = \bar{\sigma}/Y \end{aligned}\right\} \tag{4}$$

From Eqs. (3) and (4), the elastic thermal stress can be written as

$$\sigma(\xi,\tau) = -\frac{\beta}{\sqrt{\tau}}\exp\left(-\frac{\xi^2}{\tau}\right) \qquad (0 < \xi < \xi_d\,,\ 1 < \tau < \infty) \tag{5}$$

where ξ_d is the dimensionless film thickness and

$$\beta = \frac{\alpha T_o E}{(1-\nu)Y} \tag{6}$$

Here, we call β the dimensionless fluence since the surface temperature T_o after the exposure period is almost proportional to the fluence level.

We use elastoplastic thermal stress analysis[3,4] to determine the residual stress, assuming temperature-independent properties of the film material. We denote by $\sigma_{CM}(\xi)$ the maximum elastic compressive stress attainable at ξ over the entire time history. Then, it follows from Eq. (5) that the compressive stress decreases monotonically with time for $0 < \xi < 1/\sqrt{2}$ and reaches its maximum at $\tau = 2\xi^2$ for $1/\sqrt{2} < \xi < \infty$. Thus, we have

$$\left.\begin{aligned} \sigma_{CM}(\xi) &= \beta\exp(-\xi^2) \qquad (0 < \xi < 1/\sqrt{2}) \\ &= \frac{\beta e^{-1/2}}{\sqrt{2}}\cdot\frac{1}{\xi} \qquad (1/\sqrt{2} < \xi) \end{aligned}\right\} \tag{7}$$

Figure 3 shows the distribution of $\sigma_{CM}(\xi)/\beta$ and the temperature at the end of exposure period. The film remains elastic if σ_{CM} is less than unity, while yielding prevails if σ_{CM} exceeds unity. Therefore, the maximum yield depth, ξ_Y, is determined from Eq. (7) as follows:

$$\begin{aligned} \xi_Y &= \sqrt{\log\beta} \qquad (1 < \beta \le e^{1/2}) \\ \xi_Y &= \frac{e^{-1/2}}{\sqrt{2}}\beta \qquad (e^{1/2} \le \beta) \end{aligned} \tag{8}$$

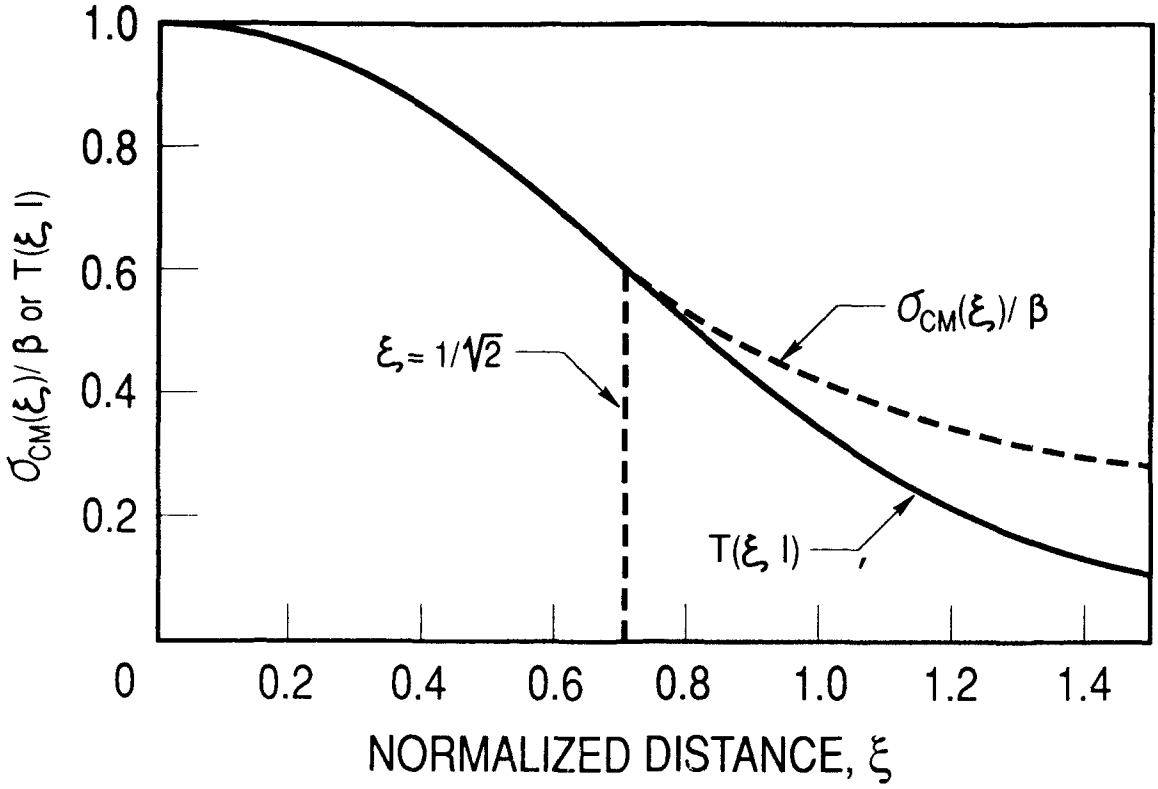

Figure 3. Temperature distribution, $T(\xi, 1)$ and $\sigma_{CM}(\xi)/\beta$.

For unloading, the elastic stress-strain relation will apply and the total relaxed stress is simply σ_{CM}. We note that the residual stress $\sigma_R(\xi)$ is the sum of σ_{CM} and the stress at the start of unloading, -1 for plastic range and $-\sigma_{CM}$ for elastic range, following Weiner's paper.[3] There is no residual stress throughout film thickness for β less than 1. For β greater than unity, the residual stress in the film is determined as follows.

A. ELASTOPLASTIC-BRITTLE MATERIAL

(a) $1 < \beta < e^{1/2}$

$$\left.\begin{aligned} \sigma_R(\xi) &= -1 + \beta \exp(-\xi^2) && \left(0 < \xi \le \sqrt{\log\beta}\right) \\ &= 0 && \left(\sqrt{\log\beta} \le \xi\right) \end{aligned}\right\} \tag{9}$$

(b) $e^{1/2} \le \beta$

$$\left.\begin{aligned} \sigma_R(\xi) &= -1 + \beta \exp(-\xi^2) && \left(0 < \xi \le 1/\sqrt{2}\right) \\ &= -1 + \frac{e^{-1/2}}{\sqrt{2}} \frac{\beta}{\xi} && \left(1/\sqrt{2} \le \xi \le \frac{e^{-1/2}}{\sqrt{2}}\beta\right) \\ &= 0 && \left(\frac{e^{-1/2}}{\sqrt{2}}\beta \le \xi\right) \end{aligned}\right\} \qquad (10)$$

Equations (9) and (10) are valid until σ_R reaches $s = S/Y$.

B. ELASTOPLASTIC MATERIAL

(a) $1 < \beta < e^{1/2}$ Same with Eq. (9)

(b) $e^{1/2} \le \beta < 2$ Same with Eq. (10)

(c) $2 \le \beta < 2e^{1/2}$

$$\left.\begin{aligned} \sigma_R(\xi) &= 1 && \left(0 < \xi < \sqrt{\log(\beta/2)}\right) \\ &= -1 + \beta \exp(-\xi^2) && \left(\sqrt{\log(\beta/2)} \le \xi < 1/\sqrt{2}\right) \\ &= -1 + \frac{e^{-1/2}}{\sqrt{2}} \frac{\beta}{\xi} && \left(1/\sqrt{2} \le \xi \le \frac{e^{-1/2}}{\sqrt{2}}\beta\right) \\ &= 0 && \left(\frac{e^{-1/2}}{\sqrt{2}}\beta \le \xi\right) \end{aligned}\right\} \qquad (11)$$

(d) $2e^{1/2} \leq \beta$

$$\left.\begin{aligned} \sigma_R(\xi) &= 1 && \left(0 < \xi < \frac{e^{-1/2}}{2\sqrt{2}}\beta\right) \\ &= -1 + \frac{e^{-1/2}}{\sqrt{2}}\frac{\beta}{\xi} && \left(\frac{e^{-1/2}}{2\sqrt{2}}\beta \leq \xi < \frac{e^{-1/2}}{\sqrt{2}}\beta\right) \\ &= 0 && \left(\frac{e^{-1/2}}{\sqrt{2}}\beta \leq \xi\right) \end{aligned}\right\} \tag{12}$$

Figure 4 shows sketches of stress distributions at the instant of the largest yield region in compression and the residual stress distributions, where ξ_Y and ξ_T denote the depths of yield region in compression and in tension, respectively. For the stress distribution at the instant of the largest ξ_Y, the unloading may already have started for β larger than $e^{1/2}$. This uncertainty is represented by a dashed curve. The tensile strength is depicted by a dash-dotted line.

If we assume that the crack appears in the region where the residual stress exceeds the normalized tensile strength s, the crack depth, ξ_c, can be determined from Eqs. (9) and (10) as follows:

(a) $0 < \beta < 1 + s$: no crack

(b) $1 + s < \beta < (1 + s)e^{1/2}$

$$\xi_c = \left[\log\left(\frac{\beta}{1+s}\right)\right]^{1/2} \tag{13}$$

(c) $(1 + s)e^{1/2} < \beta$

$$\xi_c = \frac{e^{-1/2}}{\sqrt{2}(1+s)}\beta \tag{14}$$

The crack penetrates the entire film thickness when ξ_c is larger than the normalized film thickness ξ_d, which is 1.616 for the current example in which $\kappa = 0.3$ cm^2/sec, $t_o = 22$ nsec, and $d = 2.625$ μm.

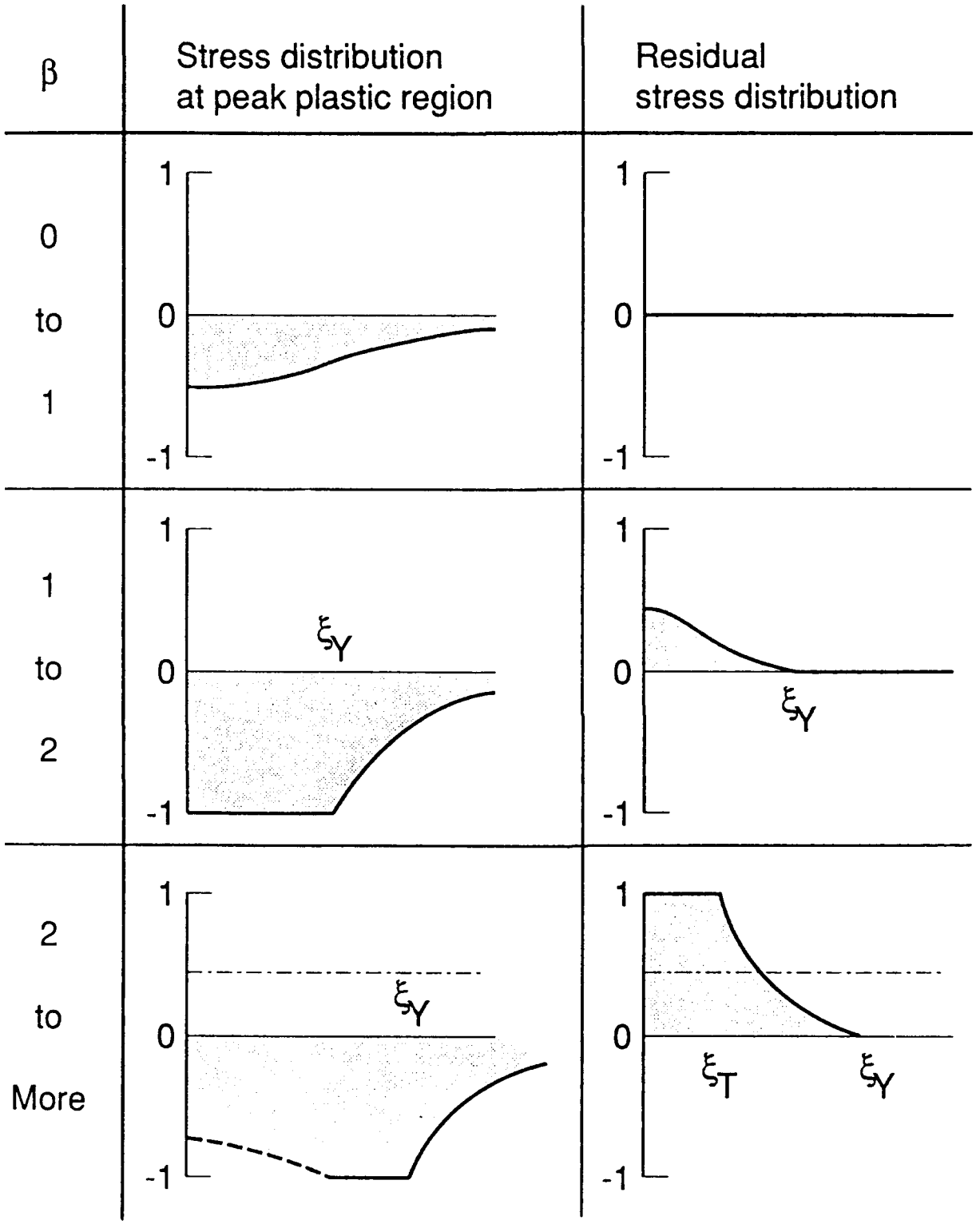

Figure 4. Schematic distribution of stress at the instant of peak compressive yield region and residual stress.

Variation of residual stress with normalized distance ξ is evaluated from Eqs. (9) and (10), and is shown for β = 1.5, 2.0, 3.0, and 4.0 in Figure 5. Here, the surface stress is $\beta - 1$ for $\beta > 0$.

Wrinkling damage mode was observed for discrete-layered coating under normalized fluence 1.70 as seen in Figure 1. Discrete-layered coating consists of distinct Si-Ge layers with a total thickness of 2.625 μm. Posttest examination of the specimen reveals no separation between the layers nor between the coating and substrate. Supported by this observation, and by the sudden temperature rise of the first few layers soon after the x-ray radiation, we regard the wrinkling phenomena as an instability of an elastic plate of thickness h under equal biaxial compression of magnitude N lying on an elastic foundation with a spring constant K.

Suppose that a bending instability of the plate causes a displacement u in the thickness direction. Then, the displacement u obeys the differential equation[5,6]

$$D\frac{d^4u}{dy4} + N\frac{d^2u}{dy2} + Ku = 0 \tag{15}$$

where y is a coordinate perpendicular to the wrinkling and

$$D = \frac{Eh^3}{12(1-\nu^2)} \tag{16}$$

To have a displacement of sinusoidal form, the compressive force N must have a critical value

$$N_{cr} = \sqrt{4KD} \tag{17}$$

For this critical compressive force, the displacement and the wavelength of wrinkling are given by

$$u(y) = C\sin\gamma y \quad , \quad \gamma = \left(\frac{K}{4D}\right)^{1/4} \tag{18}$$

and

$$\ell = \frac{2\pi}{\gamma} = 2\pi\left(\frac{4D}{K}\right)^{1/4} \tag{19}$$

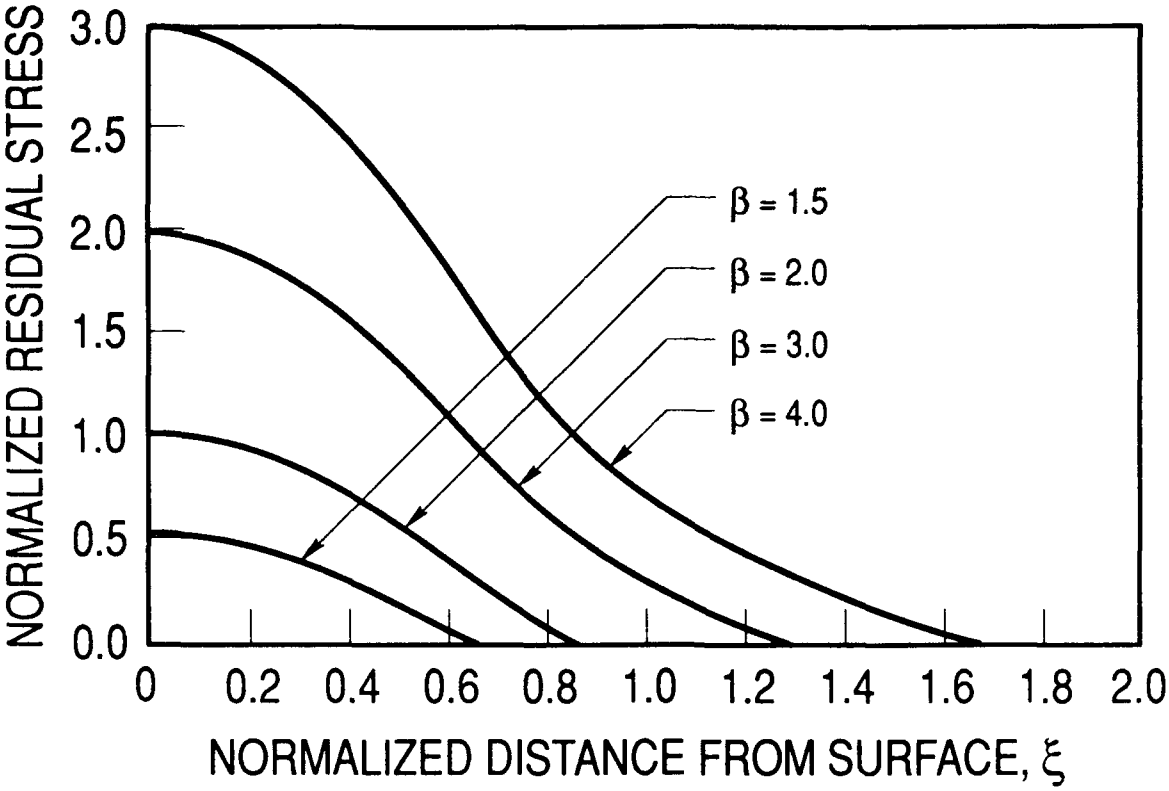

Figure 5. Residual stress distribution.

4. DAMAGE MECHANISMS

As seen in the preceding section, the parameter that determines the residual stress distribution is the dimensionless fluence β defined by Eq. (6). In the experiment, the discrete layered and rugate coatings were used, while our simplified analysis was concerned with the homogeneous film. To explain the mechanism of the damage mode in light of the analysis, we regard each of the inhomogeneous coatings as a homogeneous film with the mean values of mechanical and thermal properties.

Material properties at 200°C are chosen as follows:[7,8,9]

Si: $E = 158$ GPa, $\nu = 0.25$, $\alpha = 3 \times 10^{-6}/°C$

Ge: $E = 123$ GPa, $\nu = 0.21$, $\alpha = 6.2 \times 10^{-6}/°C$

Thus, we have

$$\left(\frac{\alpha E}{1-\nu}\right)_{\text{mean}} = \frac{1}{2}\left[\left(\frac{\alpha E}{1-\nu}\right)_{Si} + \left(\frac{\alpha E}{1-\nu}\right)_{Ge}\right] = 799 kPa/°C \tag{20}$$

The dimensionless fluence, $\beta = 1$, corresponds to the surface temperature T_o at the end of x-ray radiation which causes the yielding in compression on the surface. We assume that the surface yields at the threshold fluence given in Table 1; then, the normalized fluence used to classify the damage modes in Figure 1 can be regarded as β since the fluence and T_o are roughly proportional. Furthermore, our assumption of the equivalence between the threshold fluence and $\beta = 1$ enables us to determine the effective yield stress Y in compression by use of Table 1 and Eqs. (6) and (20) as shown in Table 2.

The first damage mode above the threshold is the defect-initiated cracking. According to the plane-strain elasticity solution[10] for a circular elastic inclusion in an elastic solid subjected to equal biaxial tension σ_o at infinity, the hoop stress at the interface decreases monotonically from $2\sigma_o$ to $2\nu\sigma_o$, as the stiffness of the inclusion increases from zero to infinity, while the radial stress at the interface increases monotonically from 0 to $2(1-\nu)\sigma_o$. For a soft inclusion, the hoop stress at the interface reaches first to the critical strength as σ_o increases and a radial crack initiates. For a stiff inclusion, the hoop stress at the interface is lower than σ_o, but the radial stress at the interface exceeds the interfacial strength, with the increase of σ_o eventually producing a debond at the interface. This corresponds to the case of a hole without inclusion. Consequently, we have a situation in which the hoop stress at the debonded interface becomes roughly twice the biaxial tension σ_o.

In view of Eqs. (9) and (10), the residual stress at the surface is found to be $\beta - 1$. For DLC/K, the defect-initiated cracking was observed for $1.33 \leq \beta \leq 1.70$ and the uniform

cracking was observed for $2.40 \leq \beta \leq 3.50$, as shown in Figure 1. Here, the lowest $\beta - 1$ value for uniform cracking, 1.40, is twice the highest $\beta - 1$ value for the defect-initiated cracking 0.70. This observation supports our argument that debonding occurs first and then the crack initiates for the defect-initiated cracking. Defect-initiated cracking can occur for $\beta - 1$ less than 0.7 since any deviation of the defect-geometry from a circular shape raises the maximum interfacial stress.

The next damage mode is wrinkling, which occurred only for DLC. In contrast to the defect-initiated cracking, this damage mode occurs during the initial period when the coating experiences high temperature and compressive stress. To apply the analysis derived in Section 3, we regard the layer material as an elastoplastic material and interpret E as the tangent modulus. Here, the compressive force N is caused by plastic deformation. Because of the predominantly plastic deformation when the instability occurs, the wrinkling remains even after the specimen cools down and the compressive force vanishes. Even though we observed that the wavelength of the wrinkling is 1.4 ~ 2 μm, we cannot draw any further information due to the lack of data on material and geometric parameters in the analytical solution.

The uniform cracking is caused by the residual tension in the coating similar to the defect-initiated cracking. We consider, in view of Figure 1, that the uniform cracking occurs when β exceeds 2.40. The surface residual stress is $\beta - 1 = 1.40$. If the crack initiates and propagates over the entire film thickness when the surface stress reaches the tensile strength, the tensile strength s follows from Eq. (4) that

$$s = 1.4\,Y \tag{21}$$

where the value of effective yield stress in compression for DLC and RC under krypton x rays is given in Table 2.

Table 2. Effective Yield Stress In Compression

Coating Type	Krypton	Argon
DLC	271 MPa	465 MPa
RC	432 MPa	508 MPa

REFERENCES

1. F. B. Sinsheimer, W. H. Childs, S. R. Gyetvay, and W. M. Graven, *Comparative Responses to Pulsed Soft X Rays of Multilayered and Compositionally Modulated (Rugate) Films,* Aerospace Report ATR-88(3783-04)-1 (November 1988).

2. H. S. Carslaw and J. C. Jaeger, *Conduction of Heat in Solids,* Clarendon Press, Oxford (1947).

3. J. Weiner, "An Elastoplastic Thermal-Stress Analysis of a Free Plate," *J. Appl. Mech.* **27**, 395 (1945).

4. B. O. Boley and J. H. Weiner, *Theory of Thermal Stresses,* John Wiley (1960); Reprinted, Robert E. Krieger, ed. (1985).

5. M. Hetényi, *Beams on Elastic Foundation,* The University of Michigan Press (1946).

6. S. Timoshenko and S. Woinowsky-Krieger, *Theory of Plates and Shells,* McGraw-Hill (1959).

7. H. J. Frost and M. F. Ashby, *Deformation-Mechanism Maps,* Pergamon Press (1982).

8. M. A. Salama, W. M. Rowe, and R. K. Yasui, *Thermoelastic Analysis of Solar Cell Arrays and their Material Properties,* Jet Propulsion Lab., JPL-TM-33-626 (1973).

9. A. K. Sinha, H. J. Levinstein, and T. E. Smith, "Thermal Stresses and Cracking Resistance of Dielectric Films (SiN, Si_3N_4, and SiO_2) on Si Substrates," *J. Appl. Phys.* **49**, 2423 (1978).

10. A. K. Mal and S. J. Singh, *Deformation of Elastic Solids,* Prentice Hall, 179 (1991).

TECHNOLOGY OPERATIONS

The Aerospace Corporation functions as an "architect-engineer" for national security programs, specializing in advanced military space systems. The Corporation's Technology Operations supports the effective and timely development and operation of national security systems through scientific research and the application of advanced technology. Vital to the success of the Corporation is the technical staff's wide-ranging expertise and its ability to stay abreast of new technological developments and program support issues associated with rapidly evolving space systems. Contributing capabilities are provided by these individual Technology Centers:

Electronics Technology Center: Microelectronics, solid-state device physics, VLSI reliability, compound semiconductors, radiation hardening, data storage technologies, infrared detector devices and testing; electro-optics, quantum electronics, solid-state lasers, optical propagation and communications; cw and pulsed chemical laser development, optical resonators, beam control, atmospheric propagation, and laser effects and countermeasures; atomic frequency standards, applied laser spectroscopy, laser chemistry, laser optoelectronics, phase conjugation and coherent imaging, solar cell physics, battery electrochemistry, battery testing and evaluation.

Mechanics and Materials Technology Center: Evaluation and characterization of new materials: metals, alloys, ceramics, polymers and their composites, and new forms of carbon; development and analysis of thin films and deposition techniques; nondestructive evaluation, component failure analysis and reliability; fracture mechanics and stress corrosion; development and evaluation of hardened components; analysis and evaluation of materials at cryogenic and elevated temperatures; launch vehicle and reentry fluid mechanics, heat transfer and flight dynamics; chemical and electric propulsion; spacecraft structural mechanics, spacecraft survivability and vulnerability assessment; contamination, thermal and structural control; high temperature thermomechanics, gas kinetics and radiation; lubrication and surface phenomena.

Space and Environment Technology Center: Magnetospheric, auroral and cosmic ray physics, wave-particle interactions, magnetospheric plasma waves; atmospheric and ionospheric physics, density and composition of the upper atmosphere, remote sensing using atmospheric radiation; solar physics, infrared astronomy, infrared signature analysis; effects of solar activity, magnetic storms and nuclear explosions on the earth's atmosphere, ionosphere and magnetosphere; effects of electromagnetic and particulate radiations on space systems; space instrumentation; propellant chemistry, chemical dynamics, environmental chemistry, trace detection; atmospheric chemical reactions, atmospheric optics, light scattering, state-specific chemical reactions and radiative signatures of missile plumes, and sensor out-of-field-of-view rejection.